Research paper

The effect of diagenesis and fluid migration on rare earth element distribution in pore fluids of the northern Cascadia accretionary margin

Ji-Hoon Kim [a,b], Marta E. Torres [b,*], Brian A. Haley [b], Miriam Kastner [c], John W. Pohlman [d], Michael Riedel [e], Young-Joo Lee [a]

[a] Petroleum and Marine Resources Research Division, Korea Institute of Geoscience and Mineral Resources, 92 Gwahang-no Yuseong-gu, Daejeon 305-350, South Korea
[b] College of Oceanic and Atmospheric Sciences, Oregon State University, Corvallis, OR 97331, USA
[c] Scripps Institution of Oceanography, University of California, San Diego, La Jolla, CA 92093, USA
[d] U.S. Geological Survey, Woods Hole Coastal & Marine Science Center, 384 Woods Hole Rd, Woods Hole, MA 02543, USA
[e] Pacific Geoscience Centre, Geological Survey of Canada, 9860 West Saanich Road, Sidney, Canada BC V8L 4B2

ABSTRACT

Analytical challenges in obtaining high quality measurements of rare earth elements (REEs) from small pore fluid volumes have limited the application of REEs as deep fluid geochemical tracers. Using a recently developed analytical technique, we analyzed REEs from pore fluids collected from Sites U1325 and U1329, drilled on the northern Cascadia margin during the Integrated Ocean Drilling Program (IODP) Expedition 311, to investigate the REE behavior during diagenesis and their utility as tracers of deep fluid migration. These sites were selected because they represent contrasting settings on an accretionary margin: a ponded basin at the toe of the margin, and the landward Tofino Basin near the shelf's edge. REE concentrations of pore fluid in the methanogenic zone at Sites U1325 and U1329 correlate positively with concentrations of dissolved organic carbon (DOC) and alkalinity. Fractionations across the REE series are driven by preferential complexation of the heavy REEs. Simultaneous enrichment of diagenetic indicators (DOC and alkalinity) and of REEs (in particular the heavy elements Ho to Lu), suggests that the heavy REEs are released during particulate organic carbon (POC) degradation and are subsequently chelated by DOC. REE concentrations are greater at Site U1325, a site where shorter residence times of POC in sulfate-bearing redox zones may enhance REE burial efficiency within sulfidic and methanogenic sediment zones where REE release ensues.

Cross-plots of La concentrations versus Cl, Li and Sr delineate a distinct field for the deep fluids (z > 75 mbsf) at Site U1329, and indicate the presence of a fluid not observed at the other sites drilled on the Cascadia margin. Changes in REE patterns, the presence of a positive Eu anomaly, and other available geochemical data for this site suggest a complex hydrology and possible interaction with the igneous Crescent Terrane, located east of the drilled transect.

© 2011 Elsevier B.V. All rights reserved.

1. Introduction

Discoveries enabled by analyses of fluids collected by scientific ocean drilling over the past decades have generated transformative changes in our understanding of the role of diagenesis and fluid flow on the biogeochemical and mechanical properties of deep-sea sediments. A growing database of major and minor elements, stable/radiogenic isotopes and, more recently, dissolved organic matter and its associated biomarkers, forms the basis for our current understanding of the roles played by fluids in subseafloor systems (e.g., Chan and Kastner, 2000; Fehn et al., 2000: Kopf et al., 2000; Brown et al., 2001; Dickens, 2001; Spivack et al., 2002; Torres et al., 2004; Teichert et al., 2005; Torres et al., 2008; Heuer et al., 2009). There are, however, only limited data on the distribution of rare earth elements (REEs) in pore fluid.

REEs comprise a set of elements with very similar chemical properties. However, the progressive filling of shielded 4f-orbital with increasing atomic number throughout the series leads to slight fractionations in their relative concentrations in natural systems. Fractionations across the series are driven by preferential complexation of the heavier REEs and preferential scavenging of the lighter REEs by particles (e.g., Sholkovitz et al., 1994). Although all the REES exist in the trivalent (3+) oxidation state, result in the anomalous oxidation states of two of its members results in a distinct behavior of Ce (Ce^{3+}, Ce^{4+}) and Eu (Eu^{2+}, Eu^{3+}) relative to other elements in the series, in response to the redox state of the system (see review by Elderfield, 1988). These characteristics make the REEs useful as tracers of geochemical processes, as their response to ligand concentrations and redox states offers valuable insights into hydrological and paleo-environmental studies.

* Corresponding author. Tel.: +1 541 737 2902; fax: +1 541 737 2064.
  E-mail address: mtorres@coas.oregonstate.edu (M.E. Torres).

To improve our understanding of REE behavior within accretionary sediments and to investigate their potential as deep fluid geochemical tracers, we have analyzed REEs in pore fluids collected up to 300 mbsf (meter below seafloor) from two sites (U1325 and U1329) drilled on the northern Cascadia margin during IODP Expedition 311. We are particularly interested in the REE response to biogeochemical transformations in reducing continental margin sediments, such as those associated with zones of methanogenesis and fermentation.

1.1. Chemical zonations in marine sediments

Redox zones in natural systems are dictated by metabolic reactions controlled by a myriad of biogeochemical processes. There is, however, an ambiguity in the current terminology used to discuss these biogeochemical redox zones in marine sediments. As outlined by Canfield and Thamdrup (2009), the presently accepted nomenclature, in particular the use of the terms "suboxic" and "anoxic", varies among researchers. These authors propose a revised scheme for classifying metabolic zones in marine sediments based on the depth distribution of common electron acceptors and the associated chemical zonations, namely: oxic, nitrogenous, manganous, ferruginous, sulfidic and methanogenic. We have adopted this nomenclature in this manuscript.

1.2. REE as geochemical tracers

The unique chemical behavior of REEs makes them powerful tracers for numerous geologic processes. For example, the variation in the REE distribution coefficients between mineral phases has been exploited to provide geologists with insights into the mode of formation of rocks (e.g., Bau and Dulski, 1996; Hofmann, 2005; Lee et al., 2010; Sugahara et al., 2010). REE analyses of lake, estuarine and seawater samples are prevalent in studies of global or local ocean circulation, redox conditions, groundwater provenance, hydrologic and hydrothermal processes (e.g., Klinkhammer et al., 1983; Hoyle et al., 1984; Ruhlin and Owen, 1986; Olivarez and Owen, 1989; Elderfield et al., 1990; Smedley, 1991; Bertram and Elderfield, 1993; Sholkovitz, 1993; German et al., 1995; Nozaki et al., 1999; Sherrell et al., 1999; Lacan and Jeandel, 2001). There is also increasing interest in the importance of REE distributions in solid phases as archives of these processes (e.g., Murray et al., 1991, 1992a, 1992b; Akagi et al., 2004; Wyndham et al., 2004; Himmler et al., 2010). Moreover, REEs can be used as tracers of release of long-lived radionuclides from nuclear waste repositories (e.g., Nitsche, 1990) and as potential indicators of environmental pollution (e.g., Olmez et al., 1991; Chiarenzelli et al., 2001; Zhang and Liu, 2004), because anthropogenic sources usually have a different REE composition relative to natural backgrounds.

REE studies in marine pore fluids, however, were limited by analytical challenges until Haley and Klinkhammer (2003) developed a technique using automated, multiple-column ion chromatography (IC) coupled with inductively coupled plasma mass spectrometry (ICP-MS). With this technique it is possible to obtain REE data from small volume samples (5 to 10 ml) of seawater and pore fluid of various compositions. Haley et al. (2004) applied this technique to samples collected from the upper 25 cm of sediments that comprise the oxic, manganous and ferruginous chemical zones. Their results show that REE concentrations exhibit a large dynamic range in these shallow sedimentary environments, and that REE fractionations reflect remineralization of organic coatings and the reduction of Fe and Ce oxides. Here we expand on these findings by analyzing pore fluids collected within sulfidic and methanogenic zones by deep-sea drilling in the northern Cascadia margin.
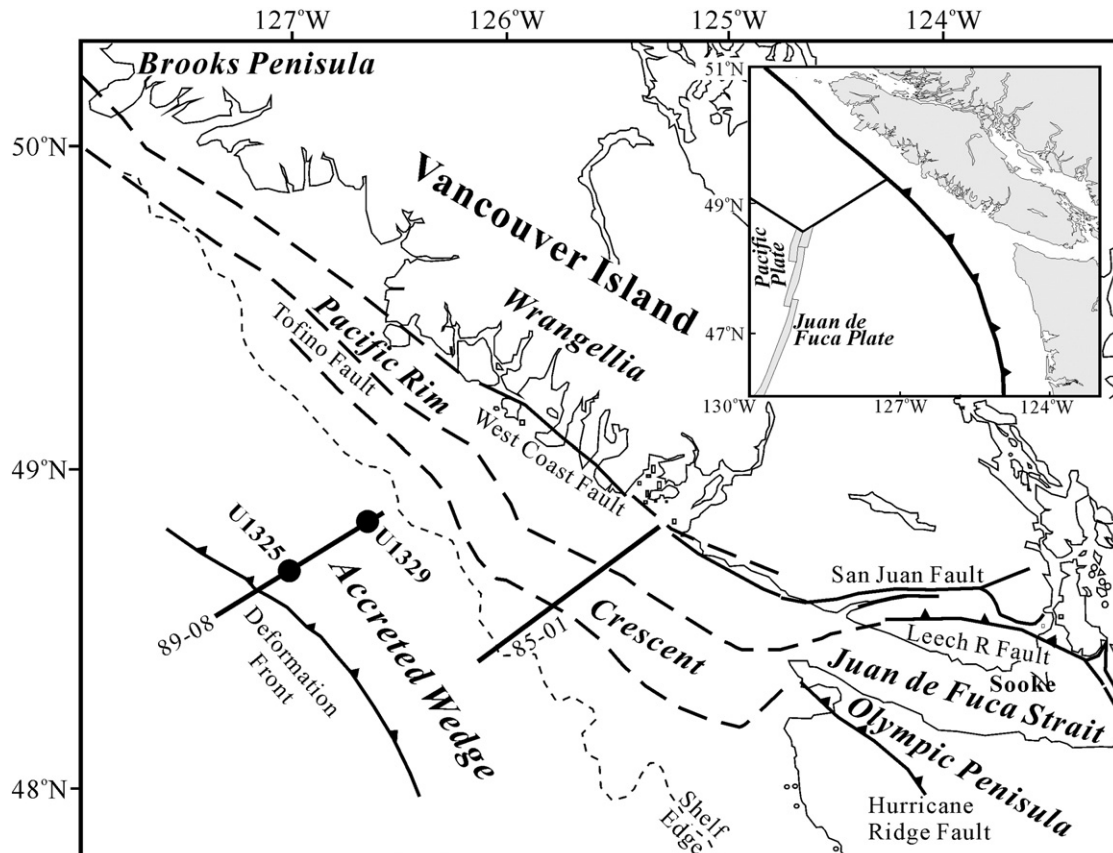

Fig. 1. Site map of the northern Cascadia margin for IODP Expedition 311.

2. Regional setting

The northern Cascadia margin accretionary complex, located offshore Vancouver Island (Canada), encompasses the modern accretionary prism and the landward Tofino Basin (Fig. 1). The Tofino Basin is a sedimentary forearc basin that formed following the accretion of the Crescent and Pacific Rim Terranes onto Wrangellia (Hayward and Calvert, 2007). It extends southeast from the Brooks Peninsula to the Juan de Fuca Strait (Narayan, 2003) and is delineated to the west by the shelf edge. The northern Cascadia accretionary prism is largely comprised of sediment that has been scraped off the subducting Juan de Fuca plate since Eocene time (~43 Ma) (Hyndman, 1995). Layered Pleistocene hemipelagic sediments are folded and faulted into anticlinal ridges at the deformation front, and further tectonic compression of the accreted material results in a landward series of folds and thrusts.

An E–W transect of four sites (U1325, U1326, U1327 and U1329) was drilled across the Cascadia margin during IODP Expedition 311 (Fig. 1). Two sites were selected for this study because they provide contrasting settings spanning most of the distance along the drilled transect, from the seaward-most slope basin ~11 km eastward of the deformation front (Site 1325) to the easternmost end of the northern Cascadia transect, at ~38 km from the deformation front (Site U1329). The seafloor in the western part of the basin drilled at Site U1325 is relatively flat with water depths around 2200 m.

Seismic data show a thick section of mostly undisturbed slope-basin type sediments with almost seafloor-parallel reflectivity (Riedel et al., 2006). The upper 50 mbsf was characterized by abundant, thick, coarse-grained (sand) layers within fine-grained (clay and silty clay) detrital sediments (Torres et al., 2008). Deeper in the section, fine-grained clay to silty clay sediments predominate, with intervals of frequent silty/sandy interlayers typical of turbidite deposition. Their frequent occurrence might indicate times of active tectonism and uplift (Riedel et al., 2006).

Site U1329 is located at a water depth of 946 m in an area characterized by multiple canyons with an average slope of 6°. Seismic data do not indicate the presence of the typical Holocene transparent layer described at the other site locations along the transect (Riedel et al., 2006). Shallow sediment (<37 mbsf) recovered by drilling at Site U1329 is dominated by clay and silty clay, locally interbedded with coarse-grained sediment. The sediment section between 37 and 136 mbsf is characterized by a high abundance of biogenic silica. A conglomerate of rounded clasts observed at 136 mbsf corresponds to an unconformity between upper Miocene and Pleistocene sediments, which can be traced seismically for several kilometers along seismic line 89–08 (Fig. 1; Riedel et al., 2006). Fine-grained detrital sediments are observed below 136 mbsf, with an increasing amount of turbidite deposition in the deeper sequences recovered. Another conglomerate was documented in the lowermost part of the drilled section (189 mbsf), possibly representing a debris flow (Riedel et al., 2006).

Table 1
REE data from pore fluid in Sites U1325 and U1329.

Site	Depth (mbsf)	La (pM)	Ce (pM)	Pr (pM)	Nd (pM)	Sm (pM)	Eu (pM)	Gd (pM)	Tb (pM)	Dy (pM)	Ho (pM)	Er (pM)	Tm (pM)	Yb (pM)	Lu (pM)	DOC (mM)
U1325	0.73	113.32	250.97	29.24	124.69	41.11	12.32	64.29	12.97	105.60	32.10	126.40	24.12	176.42	36.40	2.60
	2.93	132.88	231.56	23.81	123.23	35.07	11.66	56.82	7.93	69.25	15.16	68.27	9.04	96.80	15.38	3.93
	4.43	152.74	361.01	44.97	217.75	64.20	18.98	104.11	12.54	97.38	23.34	79.28	11.53	87.11	13.51	3.92
	5.23	187.83	410.06	44.60	217.47	49.45	12.99	77.11	10.95	69.70	21.73	68.82	13.31	112.20	19.28	4.29
	5.93	125.48	293.80	35.24	147.75	37.27	13.03	75.85	13.79	107.47	25.26	102.12	15.32	159.63	26.17	4.54
	6.73	152.36	291.28	28.77	179.44	48.93	13.34	88.76	11.52	102.46	22.68	99.56	16.90	121.72	22.75	5.27
	7.43	172.19	407.93	51.25	273.12	84.50	21.82	99.94	19.14	151.51	36.23	117.90	24.87	172.62	32.17	5.13
	26.75	41.73	101.87	12.48	69.68	13.54	5.61	29.91	7.51	97.44	42.43	187.96	40.75	359.31	77.34	—
	36.35	324.38	767.79	91.29	365.15	86.61	28.17	129.86	19.72	140.17	38.52	141.54	26.07	229.39	46.24	6.83
	45.93	117.34	240.26	29.35	145.66	40.32	11.31	69.83	12.14	99.86	38.15	152.41	30.25	272.79	54.06	7.10
	50.43	269.66	428.28	44.11	158.20	32.44	1.77	28.07	7.06	81.56	28.07	153.00	31.47	250.67	59.26	—
	55.43	74.12	183.31	29.51	127.20	28.17	8.58	53.49	13.43	92.49	22.26	80.74	16.74	113.90	19.85	6.05
	69.13	112.99	212.80	29.26	133.77	34.78	6.31	47.17	10.97	95.58	22.92	93.58	19.02	132.41	28.40	6.11
	109.76	98.56	203.54	35.62	144.47	33.84	7.20	55.77	12.68	113.23	29.93	135.04	25.32	201.66	39.15	7.71
	114.55	205.63	431.49	65.17	279.86	73.89	19.11	87.61	21.39	165.56	39.48	151.96	31.25	219.14	46.86	7.06
	249.25	96.79	74.76	13.71	60.89	22.73	11.62	53.89	4.08	43.75	12.59	43.06	7.62	60.01	10.24	4.72
	268.90	187.63	156.64	44.77	169.01	49.44	23.25	63.32	11.09	74.88	21.87	59.42	9.16	77.71	16.54	5.09
	297.80	200.62	211.23	50.97	205.33	48.38	12.82	68.28	13.26	101.84	23.25	79.48	13.47	89.32	14.48	5.88
U1329	1.45	71.16	147.74	14.81	57.13	12.16	3.78	23.19	5.33	30.46	9.85	29.55	6.22	42.47	8.83	0.45
	2.95	29.85	64.69	7.13	33.42	2.82	1.68	4.00	2.76	6.23	3.81	13.94	3.20	17.02	4.62	—
	4.45	14.84	26.82	2.60	11.97	2.60	0.59	2.43	1.01	4.34	2.70	10.59	3.17	22.31	4.63	0.92
	6.43	16.84	37.11	3.00	19.86	4.41	1.12	0.70	1.87	7.18	3.42	14.54	2.53	22.22	5.83	—
	7.93	43.03	96.08	17.84	66.99	17.48	5.94	28.60	5.82	50.29	16.82	54.57	9.45	77.29	15.61	2.09
	9.43	55.68	126.49	21.40	90.33	25.52	8.40	33.33	7.60	57.29	15.23	61.53	10.15	85.18	17.79	2.50
	10.93	63.42	139.36	19.91	74.21	27.92	8.35	34.90	10.14	80.59	27.60	119.06	22.66	193.19	45.10	—
	12.43	78.21	144.97	22.74	81.09	18.53	7.51	38.14	9.57	72.33	21.63	91.60	18.81	156.59	37.21	2.25
	13.93	93.83	196.56	28.83	115.30	35.71	14.98	56.67	13.50	111.83	30.51	116.04	20.98	157.76	33.08	—
	24.21	21.90	42.56	6.65	24.27	4.45	3.87	10.98	2.89	19.83	6.58	23.62	5.48	40.20	7.69	—
	53.53	66.74	70.07	8.29	50.63	10.62	6.59	35.82	6.19	41.94	14.42	50.55	10.01	67.18	15.00	1.80
	74.50	10.77	28.54	1.31	11.23	3.93	0.83	4.17	0.51	0.55	1.29	4.13	0.78	6.94	2.20	4.18
	89.00	50.96	80.06	8.98	51.69	13.81	3.90	20.60	3.44	19.44	7.95	22.88	5.13	39.41	8.20	4.62
	102.98	57.75	200.21	15.03	63.70	13.81	7.86	17.70	5.97	28.65	9.74	29.60	6.97	49.51	11.41	4.76
	112.50	69.85	97.34	13.53	59.92	13.06	7.76	12.82	5.28	19.23	7.71	24.25	4.20	33.30	6.67	—
	129.00	88.75	165.73	22.12	88.17	23.34	13.27	31.12	9.14	43.59	13.49	40.85	6.52	50.41	11.25	2.96
	139.95	118.18	148.38	18.66	92.31	15.40	11.97	16.26	6.23	37.15	11.13	34.49	4.36	52.57	7.97	3.04
	152.75	110.09	193.22	23.96	120.62	27.74	10.95	41.51	8.64	50.82	14.43	44.56	6.66	55.62	9.35	2.70
	176.45	99.25	153.00	20.87	97.94	19.65	9.43	25.30	7.66	53.02	14.99	43.99	7.91	56.44	9.71	—
NBP95R10[a]		56.00	22.50	7.84	33.80	6.31	1.74	8.07	1.28	9.27	2.47	7.90	1.20	8.13	1.48	—

—: not measure.

[a] Data from Haley and Klinkhammer (2003).

Table 2
REE data from sediment in Sites U1325 and U1329.

Site	Depth (mbsf)	La (μM)	Ce (μM)	Pr (μM)	Nd (μM)	Sm (μM)	Eu (μM)	Gd (μM)	Tb (μM)	Dy (μM)	Ho (μM)	Er (μM)	Tm (μM)	Yb (μM)	Lu (μM)
U1325	0.73	137.34	306.69	35.85	139.56	28.39	6.52	24.19	3.82	22.77	4.62	13.22	1.83	12.67	1.86
	2.93	146.03	300.78	36.91	145.65	29.62	6.98	24.88	3.65	23.00	4.53	12.92	1.77	12.00	1.66
	4.43	167.12	344.56	42.14	162.06	31.46	7.56	25.69	3.90	23.30	4.68	13.33	1.81	11.91	1.72
	5.23	166.64	346.10	42.12	162.10	32.37	7.61	27.10	4.02	24.87	4.81	13.75	1.95	12.67	1.89
	5.93	137.84	300.79	34.44	133.49	26.80	6.53	22.40	3.27	21.35	4.08	11.98	1.65	11.09	1.63
	6.73	150.52	322.39	37.30	143.85	28.98	6.65	23.37	3.43	21.52	4.37	12.43	1.70	11.57	1.69
	7.43	154.05	331.47	38.47	148.58	29.83	6.98	24.52	3.66	22.98	4.48	13.04	1.80	11.82	1.77
	26.75	169.85	355.40	42.38	160.95	31.12	6.73	25.03	3.67	23.02	4.59	13.22	1.80	12.17	1.76
	36.35	158.82	349.85	40.17	156.01	31.55	7.01	25.76	3.83	24.39	4.75	13.97	1.86	12.84	1.83
	45.93	156.12	330.23	40.90	161.23	33.80	7.67	27.93	4.15	26.64	5.20	14.94	2.00	13.36	1.98
	50.43	143.72	310.94	37.64	146.87	30.03	7.00	25.36	3.89	24.46	4.89	14.38	1.95	13.25	1.91
	55.43	116.96	251.19	32.06	129.25	28.27	7.43	24.63	4.03	24.08	4.89	13.55	2.04	12.52	1.99
	69.13	111.89	241.01	30.83	129.62	28.26	7.20	24.67	3.75	23.87	4.76	14.10	1.92	13.10	1.93
	109.76	139.01	303.05	36.77	145.43	30.65	7.26	25.89	4.00	24.94	4.95	14.20	1.92	13.26	1.92
	114.55	113.91	257.72	31.60	131.19	28.78	7.19	24.73	3.89	24.37	4.89	14.16	1.90	12.98	1.90
	249.25	123.40	265.62	34.34	140.30	30.94	8.15	27.88	4.35	28.53	5.60	16.17	2.21	14.91	2.18
	Average	143.33	307.36	37.12	146.01	30.05	7.15	25.25	3.83	24.01	4.76	13.71	1.88	12.63	1.85
	S.D.	19.01	36.71	3.79	11.79	1.80	0.45	1.48	0.27	1.79	0.35	1.00	0.14	0.90	0.14
U1329	1.45	150.32	315.62	36.97	144.02	29.14	7.55	24.03	3.83	23.03	4.78	12.91	1.70	11.66	1.68
	7.45	181.92	370.25	42.72	173.03	32.36	9.15	29.93	4.57	26.05	5.22	14.72	2.00	13.65	1.85
	9.55	158.59	332.96	39.10	154.57	30.41	7.16	26.19	3.92	23.19	4.71	13.24	1.95	12.35	1.85
	12.55	167.15	347.65	41.84	162.95	33.64	8.24	27.53	4.54	24.89	5.05	14.37	1.97	13.08	1.84
	23.53	177.42	361.30	43.29	166.28	32.96	8.39	28.19	4.38	23.84	5.00	13.60	1.91	12.25	1.75
	53.53	123.51	265.61	32.48	134.27	28.64	7.86	24.94	4.08	24.29	4.85	14.32	2.00	12.61	1.81
	74.50	160.09	326.94	38.54	144.96	27.43	6.80	23.43	3.73	20.48	4.13	11.91	1.52	10.08	1.44
	89.00	146.88	299.56	37.32	141.37	28.30	6.98	23.92	3.71	22.24	4.36	12.85	1.62	11.75	1.74
	102.98	150.36	323.22	38.23	146.34	29.72	7.47	24.98	3.93	23.39	4.74	14.04	1.92	12.72	1.87
	112.50	140.11	285.54	35.31	137.91	28.26	7.00	23.00	3.84	21.39	4.30	12.45	1.75	11.99	1.69
	129.00	163.64	337.79	40.13	157.42	29.72	7.79	26.62	4.13	24.51	4.81	13.92	1.97	12.42	1.96
	138.50	116.24	288.62	30.13	118.30	22.82	5.26	21.95	3.20	17.86	3.63	10.47	1.63	10.72	1.49
	152.75	135.70	303.37	34.72	138.78	27.16	6.79	22.36	3.45	21.03	4.16	11.81	1.75	11.05	1.68
	176.45	119.92	277.32	32.03	124.97	26.40	6.73	23.95	3.87	22.28	4.58	13.04	1.81	12.14	1.81
	Average	149.42	316.84	37.34	146.08	29.07	7.37	25.07	3.94	22.75	4.60	13.12	1.82	12.03	1.75
	S.D.	20.53	31.70	4.05	15.50	2.82	0.93	2.33	0.38	2.10	0.43	1.18	0.16	0.94	0.15
PAAS[a]		275.01	568.10	62.67	235.02	36.91	7.11	29.63	4.87	28.80	6.03	17.04	2.40	16.30	2.47

[a] Data from Taylor and McLennan (1985).

3. Methods

3.1. Sampling

Pore fluid was extracted from whole round samples (10 to 50 cm in length) collected immediately after retrieval of the core, using the procedure described in Riedel et al. (2006). After extrusion from the core liner, the surfaces of the sample were carefully scraped with a clean spatula to avoid contamination with drilling fluid. The clean sediments were extracted using a titanium squeezer, modified after the stainless steel squeezer of Manheim and Sayles (1974) and a laboratory hydraulic press (<20 MPa). Pore fluid was filtered through a Whatman paper and an in-line 0.20-μm Gelman® filter.

3.2. Rare earth element analysis

We selected samples from two sites U1325 ($n = 18$) and U1329 ($n = 19$) for pore fluid REE analysis. Subsamples were collected in acid-washed syringes, transferred into acid-washed Nalgene® bottles and treated with 30 ul ultra pure HNO_3 to prevent adsorption to vial walls. We used the methods for pore fluid REE analysis developed by Haley and Klinkhammer (2003). The procedure involves an automated separation and concentration of the REEs using a Dionex DX 500 high performance liquid chromatography (HPLC) followed by in-line analyses on a VG ExCell quadrupole ICP-MS at the W.M. Keck Collaboratory for Plasma Mass Spectrometry (Oregon State University). Briefly, samples (7 ml) are loaded onto a MetPac CC-1 column that retains transition elements and removes the alkali and alkaline-earth metals. The transition elements and the REEs are loaded, via an IonPac

TMC-1 column, onto a CS5A Analytical Column to separate the individual REEs. The solution eluted from the Dionex chromatograph is fed directly to the ICP-MS, which is fitted with a Teflon® BR parallel injection nebulizer (Burgener Research, Ontario, Canada). The REE concentrations (in counts per second, cps) were quantified using Time Resolved Analyses (TRA) software, and standardized against a series of REE standard solutions. Blanks were run every 5 samples. A seawater sample (NBP95R10) collected from 1300 m depth in the Bransfield Strait in the Southern Ocean (62° 46′S; 59° 24′W) was used as the in-house reference solution. The precision and accuracy, estimated from repeated analyses of the 10 ppt standard, were better than ~9% (Table I in Supplementary material).

REEs in the sediment were measured at the Korea Basic Science Institute (KBSI). Powdered squeeze cake sediments (~0.2 g) were transferred to a Teflon beaker, and digested with mixed acid (HF + HNO_3 + $HClO_4$). After digestion the solutions were evaporated on a hot plate in a draft chamber, and the dried residue was then diluted with 1% HNO_3 solution and analyzed for REEs using a Thermoelemental X-5 ICP-MS. United States Geological Survey (USGS) marine sediment reference material (MAG-1), was used as reference. This is a fine-grained, gray-brown mud with a low carbonate content from the Wilkinson Basin of the Gulf of Maine (http://minerals.cr.usgs.gov/geo_chem_stand/marine.html). Precision and accuracy calculated from repeated analysis of MAG-1 were better than 10% (Table II in Supplementary material).

The REE series is often split into light (LREE), middle (MREE) and heavy REEs (HREE), but the exact definition of each of these groups varies somewhat. For this study we assigned La to Sm to the LREE; Eu to Dy to the MREE and Ho to Lu to the HREE group.
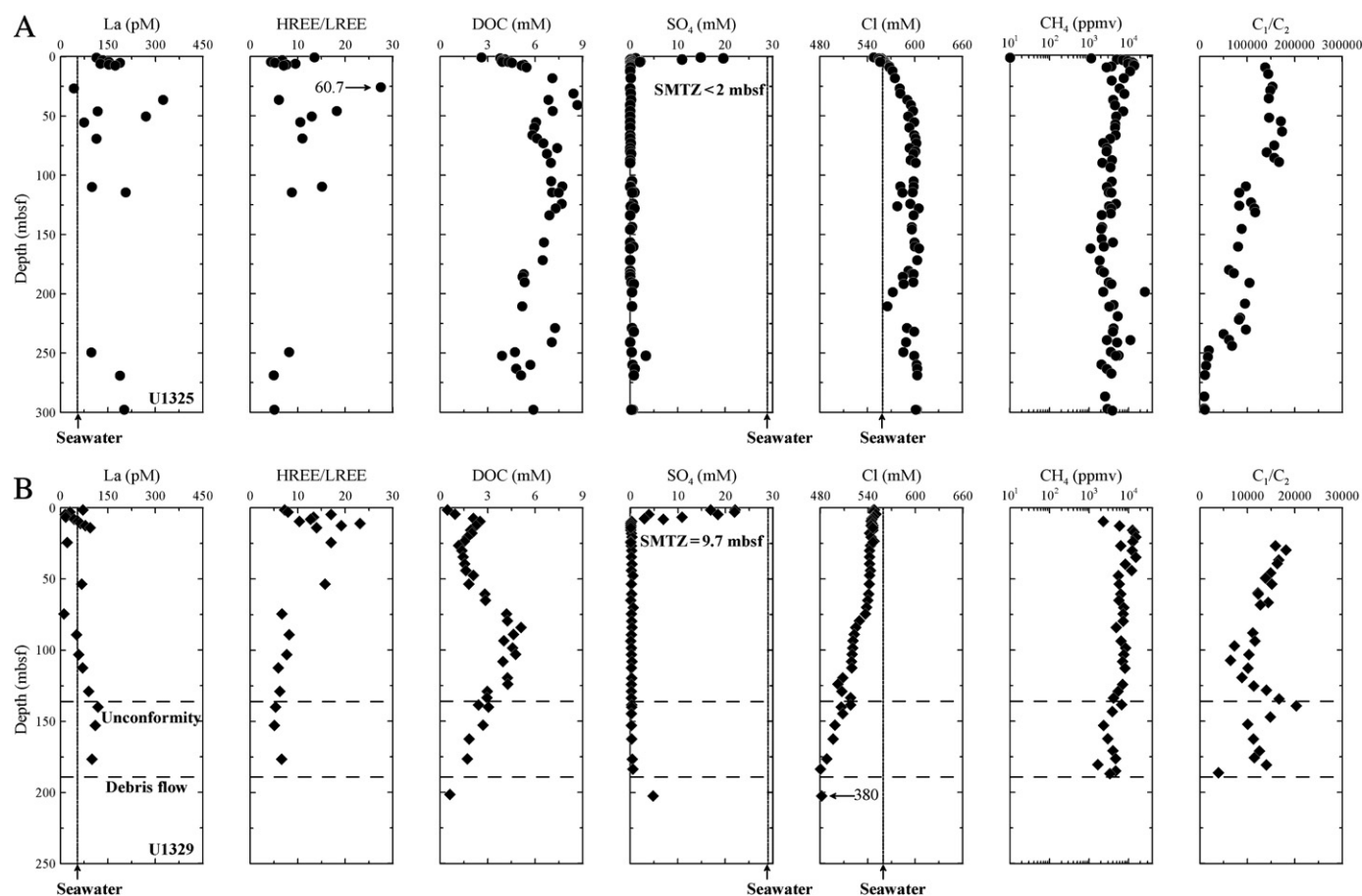
Fig. 2. Downcore profiles of La, HREE/LREE, DOC, SO_4 and Cl concentrations in pore fluid, CH_4 concentrations in headspace gasses and C_1/C_2 ratios of void gasses from A) Site U1325 (closed circles) and B) Site U1329 (closed diamonds). La concentration of seawater is from Piepgras and Jacobsen (1992); DOC, SO_4 and Cl concentrations in pore fluid, CH_4 concentrations in headspace gasses and C_1/C_2 ratios of void gasses are from the Riedel et al. (2006).

3.3. Dissolved organic carbon

Samples for DOC analysis were collected in ashed 5-ml glass ampoules and stored at −20 °C. DOC concentrations were measured using an OI Analytical 1010 TOC analyzer. Prior to DOC analysis, 5 μl of HPLC grade H_3PO_4 was added to the ampoules and the dissolved inorganic carbon (DIC) was removed by bubbling with UHP nitrogen. The DOC was oxidized to CO_2 with $Na_2S_2O_8$ in a high temperature (98 °C) reaction vessel and the CO_2 was quantified with a non-dispersive infrared detector.

4. Results

Pore fluid REE and DOC analyses are presented in Table 1; sediment REE data are listed in Table 2. The dissolved concentrations of the individual REEs are plotted against depth in Fig. I of the Supplemental material. The downcore profiles of various dissolved constituents and of methane concentrations from Riedel et al. (2006), included in Figs. 2 and II of the Supplemental material, are used to delineate and characterize the sulfidic and methanogenic zones at each site. Measured REE concentrations in the pore fluids are generally higher than seawater values (Elderfield and Sholkovitz, 1987; Sholkovitz et al., 1989; Haley et al., 2004). REE concentrations from Site U1325 are generally higher than those from Site U1329. We normalize the distribution of REEs in the sediments to Post Archean Australian Shale (PAAS; Taylor and McLennan, 1985), which show positive Eu anomalies and a depletion of LREE at both sites (see Fig. III in Supplementary material). Similar europium anomalies have been observed in red clay units recovered by ODP Sites 1215 and 1256 in the central and eastern Pacific (Ziegler et al., 2007), the

Arabian Sea (Nath et al., 1997), the Indian Ocean (Pattan et al., 1995), and elsewhere. Such anomalies have been attributed aeolian, volcanic or hydrothermal input (Elderfield, 1988), and the presence of detrital feldspar (Murray et al., 1991). More recently, Ziegler et al. (2007) showed that the patterns observed in the central and eastern Pacific reflect authigenic clay formation, rather than the presence of volcanogenic material. Although discriminating between volcanogenic, eolian and authigenic components in the Cascadia sediments is beyond the scope of this study, given the location of our study site and the sediment lithology (Riedel et al., 2006), the observed positive anomalies in the Cascadia margin sediments may also reflect volcanic input and authigenic clay formation.

The pore fluids were normalized to both PAAS and the average sediment composition from Site U1325. The resulting series display very similar patterns across the mass range, as illustrated in Fig. 3 for samples selected from three sediment depths. The REE patterns of Sites U1325 and U1329 normalized to average sediment composition were grouped into sulfidic and methanogenic zones based on the distribution of dissolved sulfate and methane in these sediments (Figs. 3, and IV and V in Supplementary material), with the sulfate methane transition zone (SMTZ) separating these zones (Figs. 2, and IV and V in Supplementary material).

5. Discussion

5.1. REE distributions and organic carbon dynamics

Haley et al. (2004) developed a biogeochemical model to explain REE distributions within different redox zones of shallow (<25 cm)
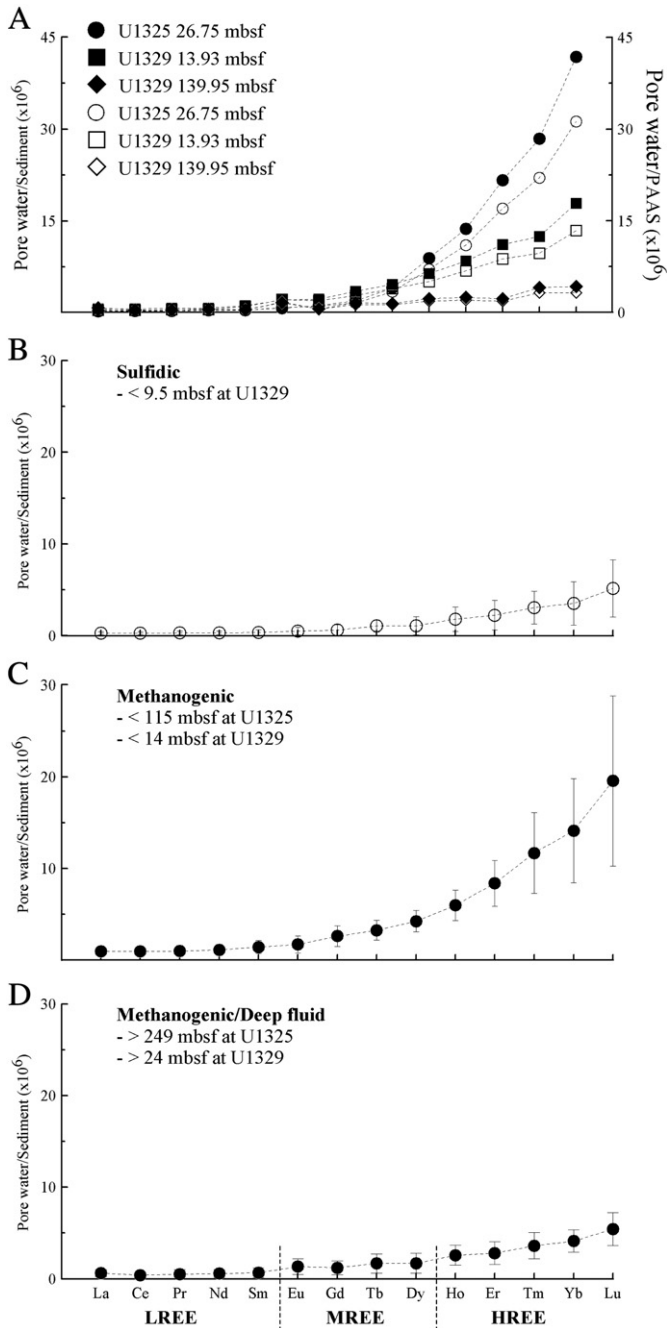
Fig. 3. A) Comparison between sediment-normalized REE patterns (closed circles) and PAAS-normalized REE patterns (open circles) for pore fluid samples from three depths at Sites U1325 and U1329. B–D) Average REE patterns normalized to the average REE values of sediment from Site U1325 for pore fluids from Sites U1325 and U1329 (error bar: 1 standard deviation). Samples from the sulfidic zone are shown with open symbols, closed symbols denote samples collected below the sulfate–methane transition zone (SMTZ).

marine sediments (Fig. 4). In their model, REEs complex with POC in surface waters and are transported to the seafloor (Sholkovitz et al., 1994; Alibo and Nozaki, 1999). Bottom water is typically enriched with HREEs because they form stronger dissolved complexes than LREEs and, as was shown by Goldberg et al. (1963), they are more effectively retained in the water column. Haley et al. (2004) show that in the oxic pore fluid of surface sediments, POC degradation preferentially releases LREEs, which produces a near-surface linear pore fluid profile. Within the ferruginous sediment zone, MREEs are released during the reduction of Fe-oxides, because Fe-oxides

precipitating in the water column efficiently and preferentially scavenge the MREEs (Haley et al., 2004). Similar bulges were reported by Himmler et al. (2010) in microcrystalline aragonite from methane seeps in the Makran prism, which they attribute to precipitation from MREE-enriched fluids close to the zone of Fe-reduction.

The model conceived by Haley et al. (2004) is also applicable to the present study. However, because of the relatively shallow depth of sulfate depletion relative to the sampled sediments (Fig. 2), all our samples come from redox zones that are deeper and more reducing than the ferrigenous and manganous zones studied by Haley et al. (2004). We therefore do not observe a MREE bulge. The sulfidic zone is sampled in the upper 9 mbsf of Site U1329, and is characterized by a flat REE pattern (open symbols in Figs. 3B and VB in Supplementary material). However, the one sample analyzed from the sulfidic zone at Site U1325 exhibits enrichment in HREE (open symbols in Fig. IVB in Supplementary material). The methanogenic zone at both studied sites displays an increase in HREE concentrations. The enrichment in HREE is consistent with a release of REEs during organic matter degradation and preferential complexation of HREEs with pore fluid dissolved metabolites (e.g., Goldberg et al., 1963; Byrne and Sholkovitz, 1996; Haley et al., 2004).

Particulate organic matter (POC) content in bulk sediments is generally higher at Site U1329 (0.80 ± 0.36 wt.%) than at Site U1325 (0.57 ± 0.31 wt.%) (Kim and Lee, 2009), but DOC concentrations are higher at Site U1325 (5.4 ± 1.4 mM) than at Site U1329 (2.7 ± 1.3 mM; Table 1, Figs. 2 and 5). Because higher DOC concentrations are expected from a more reactive POC pool, these results suggest that the amount of the DOC is not determined solely by POC concentration but by POC quality, including reactivity and generation rate. In addition, the chemical composition of POC does not show significant differences between the two sites; the average TOC/TN (8.1 ± 1.2) and $\delta^{13}C$ (-25.3 ± 1.0‰) of POC indicate fairly uniform mixture of marine and terrigenous material (Kim and Lee, 2009; Pohlman et al., 2009). Hence, the relative reactivity of POC is more likely reflected by post-depositional and diagenetic history and not by the source and amount of POC. Pohlman et al. (2009) developed a residence time model to explain how organic matter below the oxic zone at Site U1325 is likely to be more labile despite the lower concentrations. They defined the organic matter reactivity by amount of time the POC resided in the sulfate-reduction zone before being buried into methanogenic sediments. The residence time is a function of sedimentation rates and the thickness of the sulfate-bearing zones. Higher sedimentation rates and a thinner sulfate-bearing zone at Site U1325 resulted in a residence time of ~10 ka, which is an order of magnitude shorter that the residence time at Site U1329 (~100 ka). An implication of this finding is that a greater fraction of the complexed REEs was released in the sulfate-bearing zone at Site U1329, leading to lower concentrations of dissolved REEs within the deeper methanogenic zone of Site U1329 relative to those at Site U1325 (Fig. 5). Previous observations of REE release during organic matter diagenesis in the oxic zone, have shown that the LREEs are released more readily than the MREEs, followed by the HREEs, as conditions become more reducing (De Baar et al., 1988; Byrne and Kim, 1990; Stanley and Byrne, 1990; Koeppenkastrop and De Carlo, 1992; Sholkovitz, 1992; Sholkovitz et al., 1992, 1994; Schijf et al., 1995; Bau et al., 1996; Byrne and Sholkovitz, 1996; Tachikawa et al., 1999; Arraes-Mescoff et al., 2001). This behavior is then reflected in a "flattening" of the REE pattern from the HREE-enriched bottom seawater to the characteristic pattern in oxic sediment (Haley et al., 2004; Fig. 4). Lower concentrations of DOC and dissolved REEs within the deeper methanogenic zone at Site U1329 (Fig. 5) support the idea that organic matter degradation and REE loss occur in the redox zones above the sulfate-methane transition zone.

Organic matter degradation within the sulfidic and methanogenic zones releases additional DOC and REEs. Consequently, as DOC concentrations increase, so do those of the REEs (Fig. 5). The observed
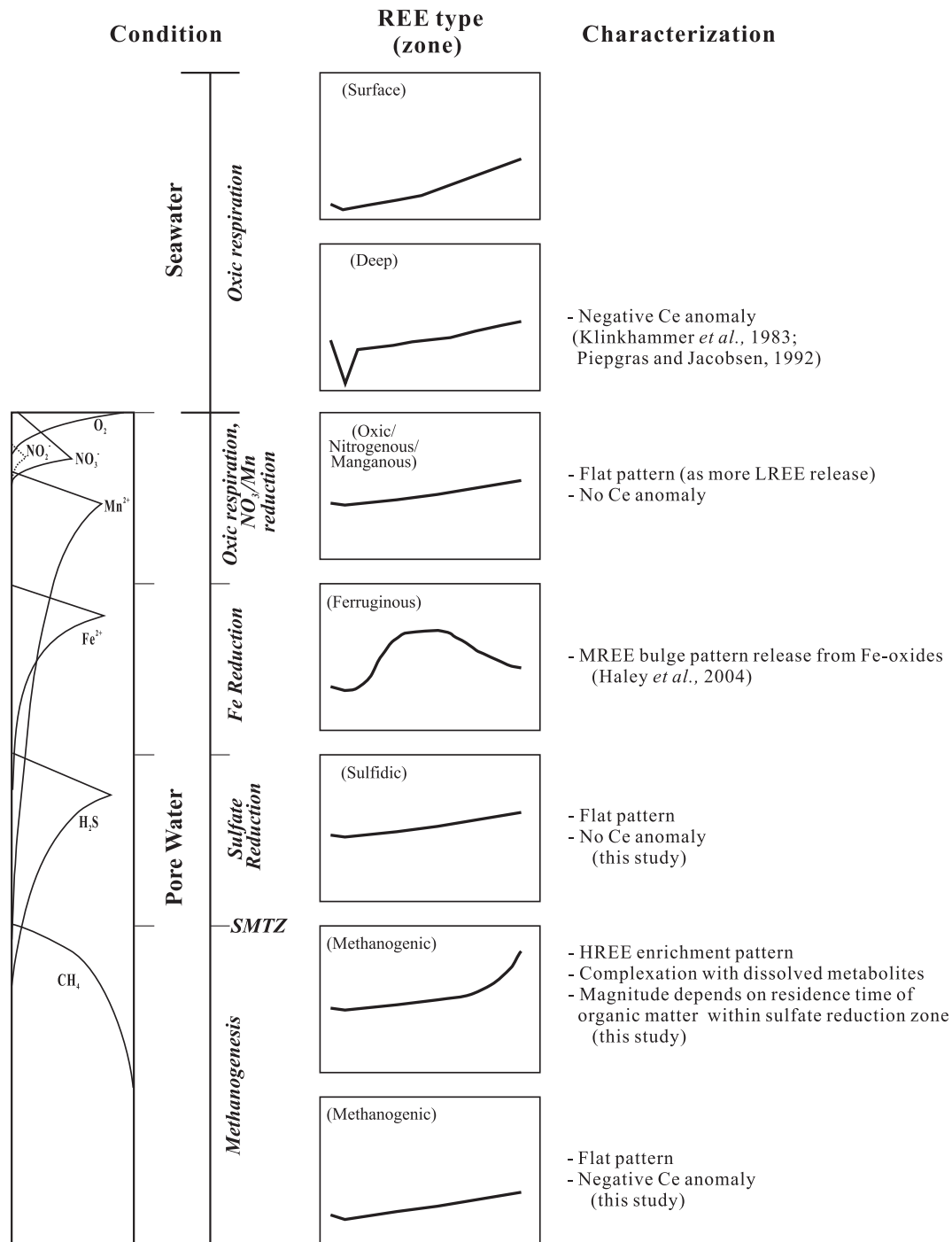
Fig. 4. Modification of the REE biogeochemical model of Haley et al. (2004) for a sample sequence that spans the range from seawater to methanogenic zone. Chemical zonation is modified from Canfield and Thamdrup (2009).

enrichment of HREEs in pore fluids at mid-depth regions (Figs. 3, and IV and V in Supplementary material) is consistent with release from an HREE-enriched organic carbon source and/or preferential complexation of the HREEs with DOC released during organic matter degradation (Haley et al., 2004). Additional REE ligands are dissolved carbonate and phosphate species (Jonasson et al., 1985; Byrne and Kim, 1993; Johannesson and Lyons, 1994; Johannesson et al., 1997; Rasmussen et al., 1998; Johannesson et al., 2000; Akagi et al., 2004; Himmler et al., 2010), which is supported by the positive correlation between REE concentration and alkalinity (a measurement of dissolved carbonate species) (Fig. 5A). There is, however, no apparent correlation with dissolved phosphate (Fig. 5A).

5.2. Cerium anomaly

Cerium tends to form the insoluble oxidized Ce^{4+} in the pe–pH range of oxic seawater, and it is thus removed from solution more effectively than the trivalent REEs. In deep oxic seawater, this behavior is evident and is generally quantified through the relationship defined as the cerium anomaly (Ce/Ce*; Bau and Dulski, 1996);

$$Ce/Ce^* = \{2Ce_N/(La_N + Pr_N)\}, \tag{1}$$

where Ce_N, La_N, Pr_N denote the sediment normalized concentrations of these REEs. Usually, negative Ce anomalies (<1) are typical of well-
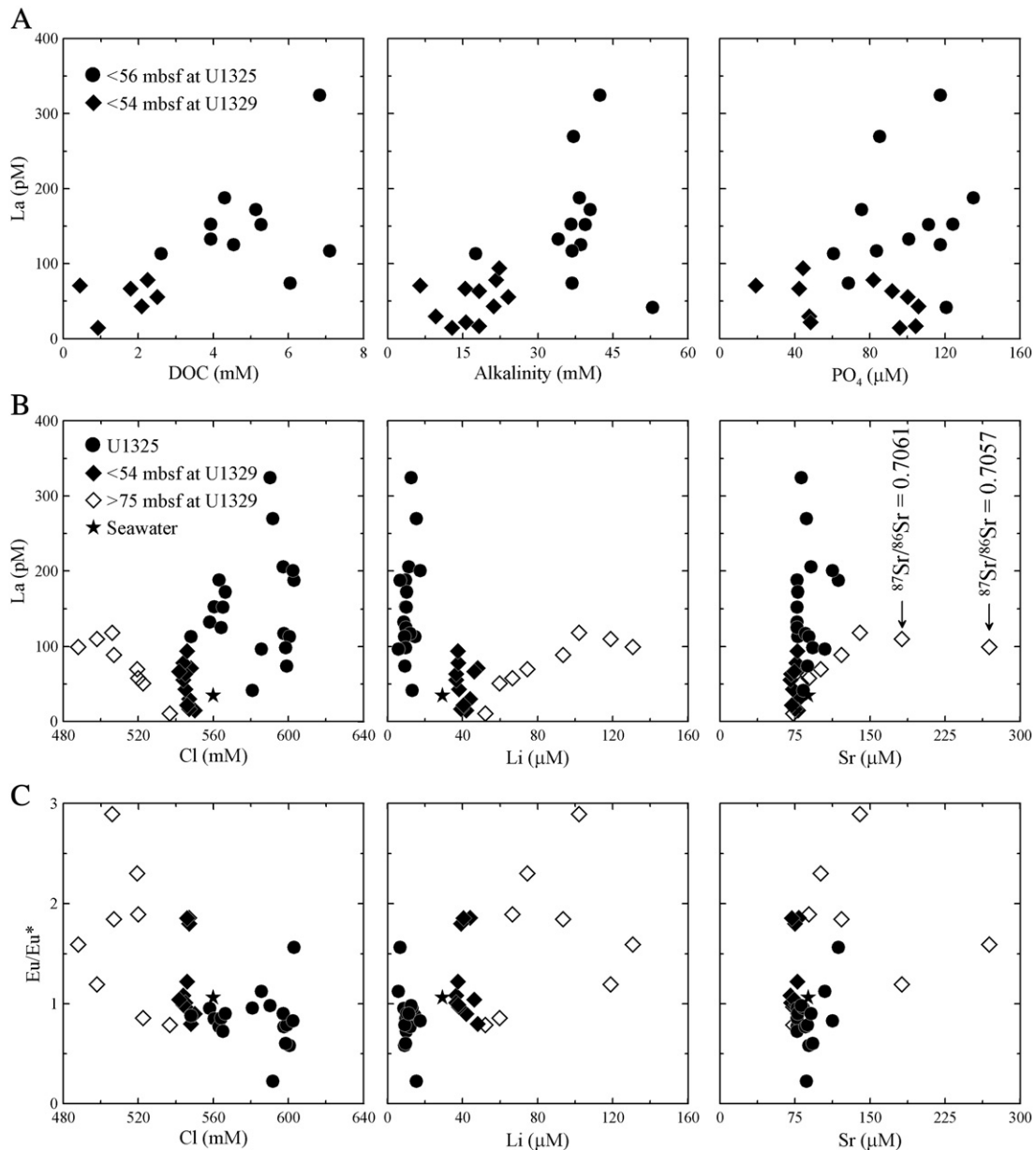
Fig. 5. A) Scatter plots of DOC, Alkalinity and PO₄ *versus* La in pore fluids from Site 1325 (closed circles) and Site U1329 (closed diamonds). Scatter plots of dissolved Cl, Li and Sr *versus* B) La and C) Eu/Eu* in pore fluid from Site 1325 (closed circles) and Site U1329 (closed diamonds: <54 mbsf, open diamonds: >75 mbsf). Seawater values are denoted by a star. $^{87}Sr/^{86}Sr$ values shown in panel B are from Riedel et al. (2010).

oxygenated seawater while positive Ce anomalies (>1) are expected under reducing conditions where soluble Ce^{3+} is more stable (Goldberg et al., 1963: Elderfield and Sholkovitz, 1987; Moffett, 1990; Sholkovitz et al., 1994). Anomalies measured in oxic seawater seem to correlate strongly with the dissolved oxygen content of the water column (Nozaki et al., 1999). Thus cerium anomalies have been used by some as indicators of redox state (Sholkovitz et al., 1992; Byrne and Sholkovitz, 1996). However, because the interpretation of apparent cerium anomalies may be hindered by anomalous abundances of La, Bau and Dulski (1996) propose the combined use of Ce and Pr anomalies, where Pr/Pr* is given by:

$$Pr/Pr^* = \{2Pr_N/(Ce_N + Nd_N)\}. \tag{2}$$

A similar approach was used here, and the results, shown in Fig. 6, corroborate our inferences based on downcore distributions of Ce/Ce*. There are apparent negative Ce anomalies in pore fluids below

50 mbsf in Site U1325 and 6 mbsf in Site U1329, which are puzzling since these pore fluids are highly reducing, *i.e.*, they correspond to the sulfidic and methanogenic redox zones (Fig. 2). Negative Ce anomalies reported in methane-seep carbonates have been ascribed to episodic oxic conditions and seawater flushing (Feng et al., 2008, 2009, 2010). This is not, however, the operating mechanism here, as seawater penetration to depths >1 mbsf is highly unlikely and not supported by other pore fluid data (Fig. 2).

An alternative explanation may be the proposed preferential uptake of dissolved Ce^{4+} by organic compounds (Pourret et al., 2008). According to these researchers, a positive Ce anomaly would develop on organic compounds, which is usually associated with high alkalinity and HREE enrichment. The pore fluids in these settings are thus expected to have a concomitant negative Ce anomaly. It seems feasible, thus, that the negative Ce anomalies observed at Sites U1325 and U1329 are another example of cerium fractionation by organic matter complexation (uptake of Ce^{4+} by DOC), rather
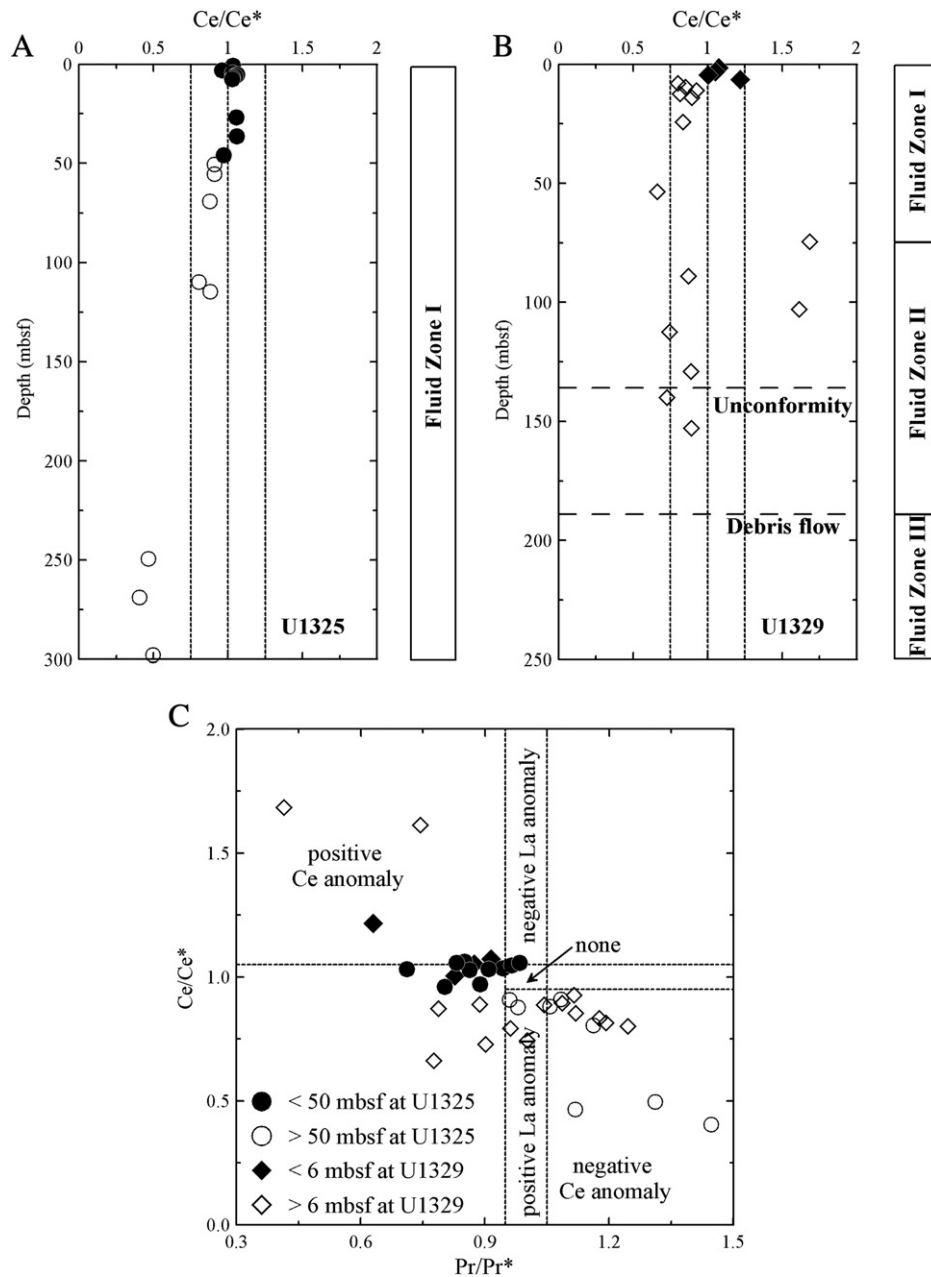
Fig. 6. Downcore profiles of Ce/Ce* from A) Site U1325 (closed circles: <50 mbsf, open circles: >50 mbsf) and B) Site U1329 (closed diamonds: <6 mbsf, open diamonds: >6 mbsf). All data are sediment-normalized REE values. C) Scatter plot of Pr/Pr* *versus* Ce/Ce* in pore fluids from Site 1325 (closed circles: <50 mbsf, open circles: >50 mbsf) and Site U1329 (closed diamonds: <6 mbsf, open diamonds: >6 mbsf). Adapted from Bau and Dulski (1996).

than oxygenation. Similarly, Himmler et al. (2010) report negative Ce anomalies in cryptocrystalline aragonite that forms in highly reducing environments at methane seeps on the Makran accretionary prism, which they also attribute to uptake of Ce^{4+} by DOC. We recognize that the evidence supporting preferential uptake of dissolved Ce^{4+} by organic compounds is limited, however, the observations of negative Ce anomalies in highly reducing fluids suggest that negative Ce anomalies may not always be a reliable proxy for paleo-oxidizing conditions.

5.3. Europium anomaly

Europium anomalies (Eu/Eu*) are calculated as (McLennan, 1989; Chavagnac et al., 2005):

$$Eu/Eu^* = \{2Eu_N/(Sm_N + Gd_N)\}, \tag{3}$$

where Eu_N, Sm_N and Gd_N denote the sediment normalized concentrations of these REEs.

Based on Eu^{3+}/Eu^{2+} equilibria in aqueous solution, MacRae et al. (1992) predict that Eu^{2+} should be highly stable at neutral to alkaline pH in strongly anoxic conditions, thus resulting in enhanced Eu abundances relative to Sm and Gd (*i.e.*, Eu/Eu*>1). Such positive europium anomalies have been reported in hydrothermal systems associated with a Ca enrichment (*e.g.*, Michard and Albarède, 1986; Michard, 1989; Klinkhammer et al., 1994; Douville et al., 1999; Craddock et al., 2010), but very little is known about the europium fractionation in highly reducing continental margin sediments, such as those associated with sulfidic and methanogenic zones. Whereas no significant Eu anomaly was observed in Site U1325 (Fig. 7A), there is a positive Eu anomaly in fluids from Site U1329 below 103 mbsf, with Eu/Eu* values ranging from 1.2 to 2.9 (2.0±0.6;

$n = 6$) (Fig. 7B). The lack of Eu anomalies in the methanogenic zone at Site U1325, indicates that even such reducing fluids do not support a significant fractionation of europium at typical chloride, temperature and pH values of continental margin sediments above 200 mbsf. The anomalies observed at Site U1329, in contrast, reflect migration of a deep-sourced fluid, as described below.

5.4. Deep fluid signatures

The dissolved Cl, Li and Sr concentrations at Site U1329 (Fig. 2) can be used to define various zones of interest at this site (Riedel et al., 2006, 2010). The marked change in slope at 75 mbsf separates the upper fluid regime from the lower ones. Cross-plots of REE concentrations versus Cl, Li and Sr delineate a distinct field for the deep fluids ($z > 75$ mbsf) from Site U1329 (open diamonds in Fig. 5), suggesting that the REE compositions of the pore fluids below 75 mbsf in this site have a component that is clearly different from fluids collected at Site U1325. Whereas the REE data at Site U1325 are controlled mostly from organic matter cycling in the sulfidic and methanogenic redox zones (Fluid Zone 1), the fluids beneath 75 mbsf at Site U1329 reflect the presence of a deep-sourced fluid, which point to a source that is clearly distinct from the rest of the fluids sampled in the accretionary margin.

The positive Eu anomalies in fluids from Site U1329 below 103 mbsf, with Eu/Eu* values ranging from 1.2 to 2.9 (2.0 ± 0.6; $n = 6$), are characteristic of REE patterns observed in high temperature hydrothermal fluids (Klinkhammer et al., 1983; Michard, 1989; Douville et al., 1999; Chavagnac et al., 2005; Craddock et al., 2010). Positive Eu anomalies appear to be restricted to high temperature, highly reducing, chloride rich solutions with pH<7 (Michard, 1989), and reflect the stability of under reducing conditions and elevated temperatures, where Eu^{2+} is expected to occur predominantly as a divalent Cl complex (Sverjensky, 1984; Allen and Seyfried, 2005). However, a comparison of fluid compositions from a variety of hydrothermal solutions showed that fluid migration through different rock types (e.g., basalt, rhyolite and sediments) does not necessarily result in different REE patterns; i.e., the REE composition in hydrothermal fluid samples does not directly mimic the REE composition of the primary crustal rocks (Michard, 1989; Craddock et al., 2010).

Because the lack of information regarding the fluid paths and source rocks feeding the deep fluids at Site U1329, we complement our REE study with other available geochemical data. In particular, the $^{87}Sr/^{86}Sr$ ratios have proven to be powerful tracers of the material
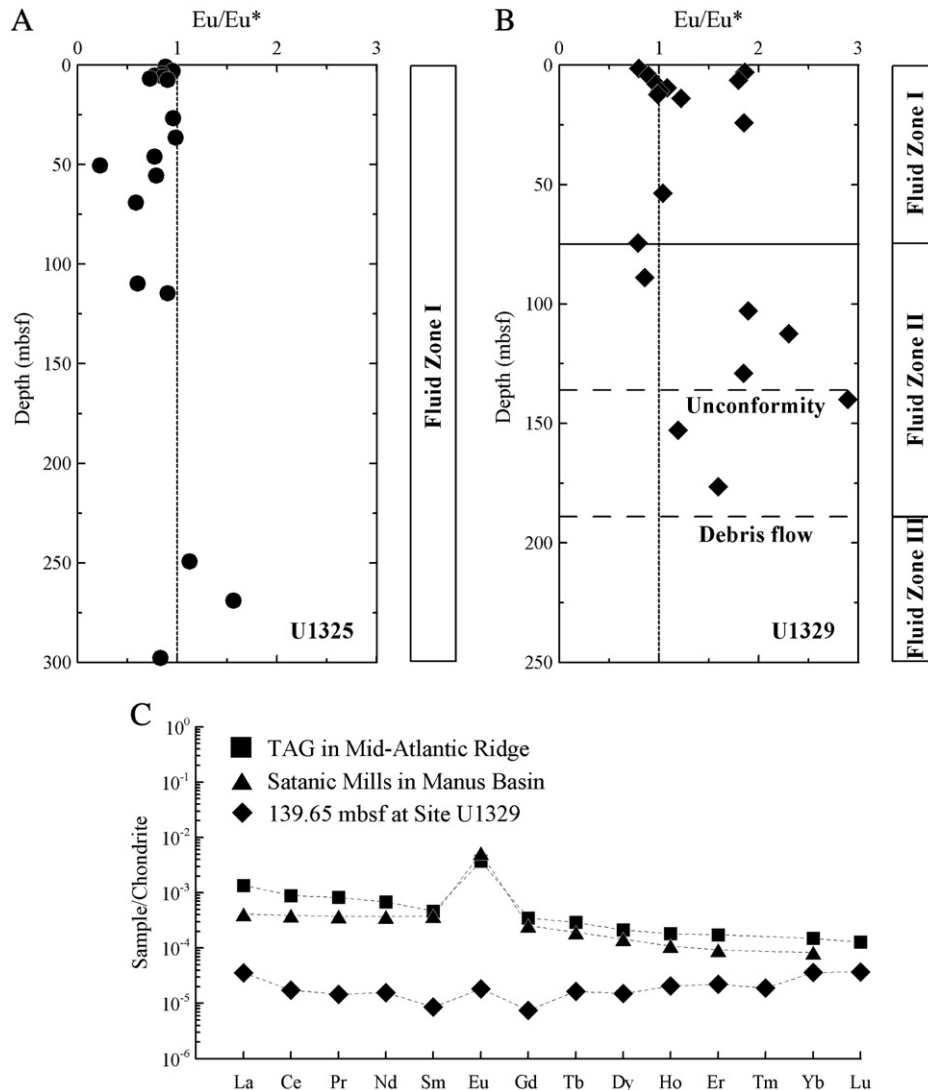

Fig. 7. Downcore profiles of Eu/Eu* from A) Site U1325 (closed circles) and B) Site U1329 (closed diamonds). C) Chondrite-normalized REE patterns of TAG hydrothermal vent in Mid-Atlantic Ridge (closed squares; Douville et al., 1999), Satanic Mills hydrothermal vent in Manus Basin (closed triangles; Craddock et al., 2010) and pore fluid from 139.65 mbsf in Site U1329 (closed diamonds).

at the fluid source. The deepest samples collected at Site U1329 have $^{87}Sr/^{86}Sr$ values of 0.7061 (162.5 mbsf) and 0.7057 (176.5 mbsf) (Riedel et al., 2010). These values are significantly lower than those measured in pore fluids collected in contact with the oceanic crust on the eastern flank of the Juan de Fuca Ridge, at ODP Site 1027B (567.98 mbsf), which have a $^{87}Sr/^{86}Sr$ value of 0.7071 (Elderfield et al., 1999). The Site 1027B deep fluids represent the oceanic end-member for the strontium isotopic composition of pore fluids in the Cascadia accretionary prism. All pore fluid samples from the central and northern Cascadia margin, except those from Site U1329, have values that span the range from seawater (0.7092) to a lowest value of 0.7072 (Teichert et al., 2005; Riedel et al., 2010), and follow the mixing curve between seawater and the oceanic end-member value from Site 1027B. The extremely low $^{87}Sr/^{86}Sr$ values measured at Site U1329 reveal that these fluids have interacted with igneous rocks that are distinct from those in the incoming oceanic crust (Joseph et al., 2011). Here we postulate that the deep-sourced fluid, which is present beneath 75 mbsf at Site U1329, reflects fluid circulation through igneous rocks of the Crescent Terrane (Fig. 8), a

Paleocene to Early Eocene oceanic assemblage of basalt flows, breccia, tuff and volcanic sandstones cut by gabbro and diabase intrusions, (Massey, 1986), derived in part from an enriched mantle source (Babcock et al., 1992; Joseph et al., 2011).

Additional data from Site U1329 indicate the presence of two distinct fluid horizons below 75 mbsf (Fluid Zones II and III), which reflect different lateral advective components to the flow regime (Fig. 8). The first horizon lies between 130 and 140 mbsf, as marked by distinct discontinuities in the dissolved Cl and K concentrations, as well as by an increase in methane to ethane (C_1/C_2) ratio. This zone lies directly underneath the bottom of the gas hydrate stability zone and straddles a 1 m conglomerate deposit (134.8 to 135.8 mbsf), which corresponds to a stratigraphic hiatus. The deepest sample from Hole U1329C (189 mbsf) recovered a 1 m thick conglomerate deposit in a pressure core (U1329C-23P), which suggests a debris flow deposit (Riedel et al., 2005). Only one sample was recovered from Hole 1329D, at 210.5 mbsf, with extremely anomalous chemical composition, suggesting that in spite of an overall porosity decrease, the region between 190 and 211 mbsf, hosts discrete
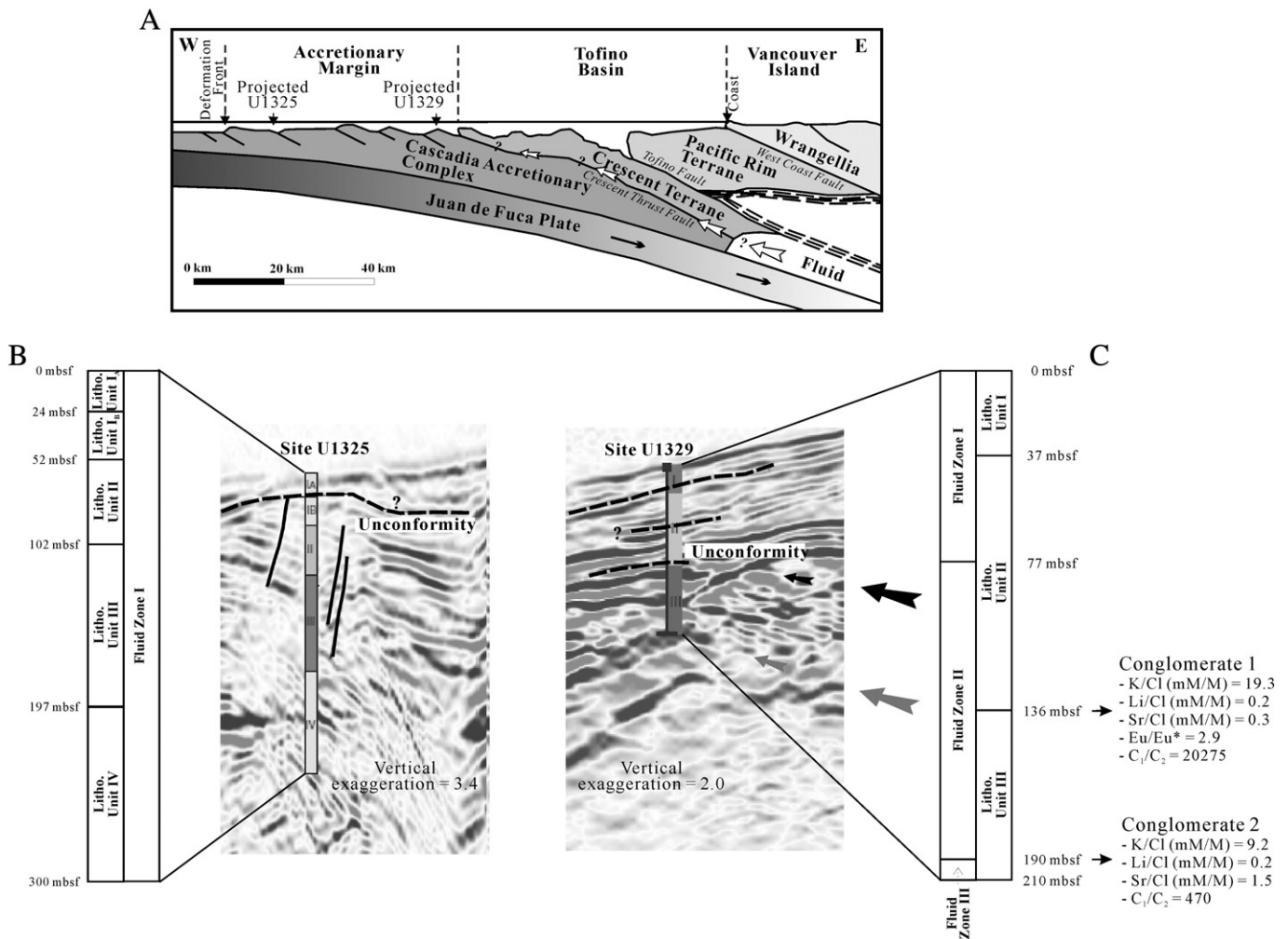

Fig. 8. A) A cross section of the northern Cascadia margin modified from Hyndman et al. (1990) and Johns et al. (2006). B) Summary of the lithologic units and fluid zones defined for Site U1325. Seismic section from MCS Line 89-08 with overlay of stratigraphic units from Riedel et al. (2005). The boundary between lithologic Unit I_A and Unit I_B is traceable for ~1.5 km around Site U1325. Several small-scale faults are visible, one of which was most likely penetrated at Site U1325 near the base of lithologic Unit II (Riedel et al., 2006). C) Summary of the lithologic units and fluid zones defined for Site U1329, showing locations of anomalous fluids associated with conglomerates recovered at the boundary between lithologic Units II and III (136 mbsf), which also define a major unconformity, and from the deepest sample recovered, at 189 mbsf. Fluid chemistry in these three horizons is very distinct and suggests a complex hydrologic regime with multiple migration paths and source fluids. Seismic section from MCS Line 89-08 with overlay of stratigraphic units from Riedel et al. (2005). The base of Unit II may be correlated to a shallow reflector that can be traced across the entire section. Another reflector, imaged at ~75 mbsf corresponds to our Fluid Zone I–II boundary, as defined by the geochemical data. Chemical compositions in Fluid Zone II indicate highly reducing fluids with a component of fluids altered by reaction with oceanic crust, possibly the Crescent Terrane. The boundary between lithologic Units II and III is an unconformity, which can be traced seismically for several kilometers along MCS Line 89-08 (Riedel et al., 2006).

horizons (possibly associated with debris flow deposits) that support lateral fluid flow, and are isolated from the sediment column by low permeability zones (possibly associated with cemented sediment). The fluid sampled from the deeper conglomerate is distinct from that at 130–140 mbsf, in that Cl and K show a marked decrease, C_1/C_2 ratios are substantially lower, and the concentrations of C_2–C_5 gasses are an order of magnitude greater than in the sample above conglomerate (Riedel et al., 2005). Insufficient pore fluid was recovered from the deepest sample for REE analyses.

Even though we lack a full data set to fully characterize the deep hydrological regime at Site U1329, the available data indicate the presence of multiple flow pathways. In general, the deep-seated fluids are likely to be under highly reducing conditions and include a component of the fluid that has reacted with igneous crust (as evidenced by positive Eu anomalies, high Li and low $^{87}Sr/^{86}Sr$ values). The possibility exists that the deep fluids at this site reflect reactions with igneous Crescent Terrane sequences, located less than 10 km away from the Site U1329. These altered fluids migrate to the drilled site along various thrust faults, such as those imaged in the seismic data of Hyndman et al. (1990) and Hyndman (1995), and other high permeability horizons, such as the sampled conglomerates.

6. Conclusions

Our results extend the understanding of REE behavior to highly reducing environments typical of the sulfate-depleted methanogenic regions sampled along continental margins worldwide. In these reducing settings, the pore fluid REEs are enriched in HREEs, a likely result of preferential complexation by organic matter metabolites, such as DOC. REE has higher values in Site U1325 than Site U1329. Sediments at Site U1329 have experienced a longer residence time in the sulfate-bearing sections of the sediment column (Pohlman et al., 2009), such that a larger fraction of the REE complexed with the organic carbon was released before burial within the sulfate depleted zone. Thus, the residence time of organic matter in the sulfate-bearing region, and not just POC concentration, is an important factor on the behavior of REEs during diagenetic processes in the methanogenic zone.

Whereas the REE distributions at Site U1325 and in the upper 75 mbsf of Site U1329 are controlled mostly by organic matter cycling in the sulfidic and methanogenic redox zones (Fluid Zone 1), the deep samples from Site U1329 reflect the presence of deep-sourced fluids, clearly distinct from the rest of the fluids sampled in the accretionary Cascadia margin. The REEs show overall good correlations with dissolved Cl, Li and Sr concentrations, and delineate the deeper fluids as a separate regime. Geochemical data from Site U1329 (Riedel et al., 2006, 2010) suggest the presence of two additional fluid flow zones below 75 mbsf. Chemistry in Fluid Zones II and III reveals a complex hydrology, with possible migration of deep fluids along various pathways. These deep-sourced fluids have a positive Eu anomaly, high Li and Sr concentrations, and $^{87}Sr/^{86}Sr$ values that are significantly lower than those measured in fluids sampled within other sites drilled in this accretionary prism. We postulate that at least a component of these deep fluids has reacted with 52–57 Ma oceanic igneous Crescent Terrane sequences, and migrated to the drill site through deep-seated faults and higher permeability pathways, perhaps associated with discrete high permeability horizons that are isolated from the rest of the sediment column by less permeable zones.

Supplementary materials related to this article can be found online at doi:10.1016/j.chemgeo.2011.10.010.

Acknowledgments

References

Akagi, T., Hashimoto, Y., Fu, F.-F., Tsuno, H., Tao, H., Nakano, Y., 2004. Variation of the distribution coefficients of rare earth elements in modern coral-lattices: species and site dependencies. Geochimica et Cosmochimica Acta 68, 2265–2273. doi:10.1016/J.GCA.2003.12.014.

Alibo, D.S., Nozaki, Y., 1999. Rare earth elements in seawater: particle association, shale-normalization and Ce oxidation. Geochimica et Cosmochimica Acta 63, 363–372.

Allen, D.E., Seyfried Jr., W.E., 2005. REE controls in MOR hydrothermal systems: an experimental study at elevated temperature and pressure. Geochimica et Cosmochimica Acta 69, 675–683.

Arraes-Mescoff, R., Roy-Barman, M., Coppola, L., Souhaut, M., Tachikawa, K., Jeandel, C., Sempere, R., Yoro, C., 2001. The behavior of Al, Mn, Ba, Sr, REE and Th isotopes during in vitro degradation of large marine particles. Marine Chemistry 73, 1–19.

Babcock, R.S., Burmester, R.F., Engebretson, D.C., Warnock, A., Clark, K.P., 1992. A rifted margin origin for the crescent basalts and related rocks in the northern coast range volcanic province, Washington and British Columbia. Journal of Geophysical Research 97, 6799–6821.

Bau, M., Dulski, P., 1996. Distribution of yttrium and rare earth elements in the Penge and Kuruman iron-formations, Transvaal Supergroup, South Africa. Precambrian Research 79, 37–55.

Bau, M., Koschinsky, A., Dulski, P., Hein, J.R., 1996. Comparison of the partitioning behaviours of yttrium, rare earth elements, and titanium between hydrogenetic marine ferromanganese crusts and seawater. Geochimica et Cosmochimica Acta 60, 1709–1725.

Bertram, C.J., Elderfield, H., 1993. The geochemical balance of the rare earth elements and neodymium isotopes in the oceans. Geochimica et Cosmochimica Acta 75, 1957–1986.

Brown, K.V., Saffer, D.M., Bekins, B.A., 2001. Smectite diagenesis, pore-water freshening, and fluid flow at the toe of the Nankai wedge. Earth and Planetary Science Letters 194, 97–109.

Byrne, R.H., Kim, K.-H., 1990. Rare earth element scavenging in seawater. Geochimica et Cosmochimica Acta 54, 2645–2656.

Byrne, R.H., Kim, K.-H., 1993. Rare earth precipitation and coprecipitation behaviour: the limiting role of PO_4^{3-} on dissolved rare earth concentrations in seawater. Geochimica et Cosmochimica Acta 57, 519–526.

Byrne, R.H., Sholkovitz, E.R., 1996. Marine chemistry and geochemistry of the lanthanides. In: Gschneidner Jr., K.A., Eyring, L. (Eds.), The Handbook on the Physics and Chemistry of the Rare Earths. Elsevier, Amsterdam, Netherlands, pp. 497–593.

Canfield, D.E., Thamdrup, B., 2009. Towards a consistent classification scheme for geochemical environments, or, why we wish the term 'suboxic' would go away. Geobiology 7, 385–392.

Chan, L.H., Kastner, M., 2000. Lithium isotopic compositions of pore fluids and sediments in the Costa Rica subduction zone: implications for fluid processes and sediment contribution to the arc volcanoes. Earth and Planetary Science Letters 183, 275–290.

Chavagnac, V., German, C.R., Milton, A., Palmer, M.R., 2005. Sources of REE in sediment cores from the Rainbow vent site (36° 14′N, MAR). Chemical Geology 216, 329–352. doi:10.1016/j.chemgeo.2004.11.015.

Chiarenzelli, J., Aspler, L., Dunn, C., Cousens, B., Ozarko, D., Powis, K., 2001. Multi-element and rare earth element composition of lichens, mosses, and vascular plants from the Central Barrenlands, Nunavut, Canada. Applied Geochemistry 16, 245–270.

Craddock, P.R., Bach, W., Seewald, J.S., Rouxel, O.J., Reeves, E., Tivey, M.K., 2010. Rare earth element abundances in hydrothermal fluids from the Manus Basin, Papua New Guinea: indicators of sub-seafloor hydrothermal processes in back-arc basins. Geochimica et Cosmochimica Acta 74, 5494–5513.

De Baar, H.J.W., German, C.R., Elderfield, H., Van Gaans, P., 1988. Rare earth element distributions in anoxic waters of the Cariaco Trench. Geochimica et Cosmochimica Acta 52, 1203–1219.

Dickens, G.R., 2001. Sulfate profiles and barium fronts in sediment on the Blake Ridge: present and past methane fluxes through a large gas hydrate reservoir. Geochimica et Cosmochimica Acta 65, 529–543.

Douville, E., Bienvenu, P., Charlou, J.L., Donval, J., Fouquet, Y., Appriou, P., Gamo, T., 1999. Yttrium and rare earth elements in fluids from various deep-sea hydrothermal systems. Geochimica et Cosmochimica Acta 63, 627–643.

Elderfield, H., 1988. The oceanic chemistry of rare-earth elements. Philosophical Transactions of the Royal Society of London 325, 105–126.

Elderfield, H., Sholkovitz, E.R., 1987. Rare earth elements in the pore waters of reducing nearshore sediments. Earth and Planetary Science Letters 82, 280–288.

Elderfield, H., Upstill-Goddard, R., Sholkovitz, E.R., 1990. The rare earth elements in rivers, estuaries and coastal sea waters and their significance to the composition of seawater. Geochimica et Cosmochimica Acta 54, 971–991.

Elderfield, H., Wheat, C.G., Mottl, M.J., Monnin, C., Spiro, B., 1999. Fluid and geochemical transport through oceanic crust: a transect across the eastern flank of the Juan de Fuca Ridge. Earth and Planetary Science Letters 172, 151–165.

Fehn, U., Synder, G., Egeberg, P.K., 2000. Dating of pore waters with [129]I: relevance for the origin of marine gas hydrates. Science 289, 2332–2335.

Feng, D., Chen, D.F., Roberts, H.H., 2008. Sedimentary fabrics in the authigenic carbonates from Bush Hill: implication for seabed fluid flow and its dynamic signature. Geofluids 8, 301–310.

Feng, D., Harry, D.C., Roberts, H., 2009. Petrographic and geochemical characterization of seep carbonate from Bush Hill (GC 185) gas vent and hydrate site of the Gulf of Mexico. Marine and Petroleum Geology 26, 1190–1198. doi:10.1016/j.marpetgeo.2008.07.001.

Feng, D., Chen, D., Peckmann, J., Bohrmann, G., 2010. Authigenic carbonates from methane seeps of the northern Congo fan: microbial formation mechanism. Marine and Petroleum Geology 27, 748–756. doi:10.1016/j.marpetgeo.2009.08.006.

German, C.R., Masuzawa, T., Greaves, M.J., Elderfield, H., Edmond, J.M., 1995. Dissolved rare earth elements in the Southern Ocean: cerium oxidation and the influence of hydrography. Geochimica et Cosmochimica Acta 59, 1551–1558.

Goldberg, E.D., Koide, M., Schmitt, R.A., Smith, R.H., 1963. Rare-earth distributions in the marine environment. Journal of Geophysical Research 68, 4209–4217.

Haley, B.A., Klinkhammer, G.P., 2003. Complete separation of rare earth elements from small volume seawater samples by automated ion chromatography: method development and application to benthic flux. Marine Chemistry 82, 197–220.

Haley, B.A., Klinkhammer, G.P., McManus, J., 2004. Rare earth elements in pore waters of marine sediments. Geochimica et Cosmochimica Acta 68, 1265–1279.

Hayward, N., Calvert, A.J., 2007. Seismic reflection and tomographic velocity model constraints on evolution of Tofino forearc basin, British Columbia. Geophysical Journal International 168, 634–643.

Heuer, V.B., Pohlman, J.W., Torres, M.E., Elvert, M., Hinrichs, K.-W., 2009. The stable carbon isotope biogeochemistry of acetate and other dissolved carbon species in deep subseafloor sediments at the northern Cascadia Margin. Geochimica et Cosmochimica Acta 73, 3323–3336. doi:10.1016/j.gca.2009.03.001.

Himmler, T., Bach, W., Bohrmann, G., Peckmann, J., 2010. Rare earth elements in authigenic methane-seep carbonates as tracers for fluid composition during early diagenesis. Chemical Geology 277, 126–136. doi:10.1016/j.chemgeo.2010.07.015.

Hofmann, A., 2005. The geochemistry of sedimentary rocks from the Fig Tree Group, Barberton greenstone belt: implications for tectonic, hydrothermal and surface processes during mid-Archaean times. Precambrian Research 143, 23–49. doi:10.1016/j.precamres.2005.09.005.

Hoyle, J., Elderfield, H., Gledhill, A., Greaves, M., 1984. The behaviour of the rare earth elements during mixing of river and sea waters. Geochimica et Cosmochimica Acta 48, 143–149.

Hyndman, R.D., 1995. The Lithoprobe corridor across the Vancouver Island continental margin: the structural and tectonic consequences of subduction. Canadian Journal of Earth Sciences 32, 1777–1802.

Hyndman, R.D., Yorath, C.J., Clowes, R.M., Davis, E.E., 1990. The Northern Cascadia Subduction Zone at Vancouver Island-seismic structure and tectonic history. Canadian Journal of Earth Sciences 27, 313–329.

Johannesson, K.H., Lyons, W.B., 1994. The rare earth element geochemistry of Mono Lake water and the importance of carbonate complexing. Limnology and Oceanography 39, 1141–1154.

Johannesson, K.H., Stetzenbach, K.J., Hodge, V.F., 1997. Rare earth elements as geochemical tracers of regional groundwater mixing. Geochimica et Cosmochimica Acta 61, 3605–3618.

Johannesson, K.H., Zhou, X., Guo, C., Stetzenbach, K.J., Hodge, V.F., 2000. Origin of rare earth element signatures in groundwaters of circumneutral pH from southern Nevada and eastern California, USA. Chemical Geology 164, 239–257.

Johns, M.J., Barnes, C.R., Narayan, Y.R., 2006. Cenozoic ichthyolith biostratigraphy: Tofino Basin, British Columbia. Canadian Journal of Earth Sciences 43, 177–204 10.1139/E05-102.

Jonasson, R., Bancroft, G., Nesbitt, H., 1985. Solubilities of some hydros REE phosphates with implications for diagenesis and seawater concentrations. Geochimica et Cosmochimica Acta 49, 2133–2139.

Joseph, C., Torres, M., Martin, R., Rose, K., Pohlman, J., Riedel, M., 2011. Methane sources, fluid flow, and diagenesis along the northern Cascadia Margin; using the carbonate record to link modern fluid flow to the past. AGU, San Francisco, Califonia.

Kim, J.-H., Lee, Y.-J., 2009. Data report: elemental, rock-eval, and isotopic compositions of bulk sediments, IODP Expedition 311. In: Riedel, M., Collett, T.S., Malone, M.J., the Expedition 311 Scientists (Eds.), Proceedings of the Integrated Ocean Drilling Program Expedition, 311. Integrated Ocean Drilling Program International Inc, Washington D.C.. doi:10.2204/iodp.proc.311.207.2009.

Klinkhammer, G., Elderfield, H., Hudson, A., 1983. Rare earth elements in seawater near hydrothermal vents. Nature 305, 185–188.

Klinkhammer, G., Elderfield, H., Edmond, J.M., Mitra, A., 1994. Geochemical implications of rare earth element patterns in hydrothermal fluids from mid-ocean ridges. Geochimica et Cosmochimica Acta 58, 5105–5113.

Koeppenkastrop, D., De Carlo, E.H., 1992. Sorption of rare-earth elements from seawater onto synthetic mineral particles: an experimental approach. Chemical Geology 95, 251–263.

Kopf, A., Deyhle, A., Zuleger, E., 2000. Evidence for deep fluid circulation and gas hydrate dissociation using boron and boron isotopes of pore fluids in forearc sediments from Costa Rica (ODP Leg 170). Marine Geology 167, 1–28.

Lacan, F., Jeandel, C., 2001. Tracing Papua New Guinea imprint on the central equatorial Pacific Ocean using neodymium isotopic compositions and rare earth element patterns. Earth and Planetary Science Letters 186, 497–512.

Lee, S.G., Asahara, Y., Tanaka, T., Kim, N.H., Kim, K.H., Yi, K., Masuda, A., Song, Y.S., 2010. La–Ce and Sm–Nd isotopic systematics of early Proterozoic leucogranite with tetrad REE pattern. Chemical Geology 276, 360–373. doi:10.1016/j.chemgeo.2010. 07.003.

MacRae, N.D., Nesbitt, H.W., Kronberg, B.I., 1992. Development of a positive Eu anomaly during diagenesis. Earth and Planetary Science Letters 109, 585–591.

Manheim, F.T., Sayles, F.L., 1974. Composition and origin of interstitial waters of marine sediments, based on deep sea drill cores. In: Goldberg, E.D. (Ed.), Marine chemistry: the sedimentary cycle. : The Sea, vol. 5. Wiley, New York, pp. 527–568.

Massey, N.W.D., 1986. Metchosin Igneous Complex, southern Vancouver Island: ophiolite stratigraphy developed in an emergent island setting. Geology 14, 602–605.

McLennan, S.M., 1989. Rare earth elements in sedimentary rocks: influence of provenance and sedimentary processes. In: Lipin, B.R., McKay, G.A. (Eds.), Geochemistry and mineralogy of rare earth elements: Mineral. Soc. Am. Rev. Mineral., 21, pp. 147–167 (Washington D.C.).

Michard, A., 1989. Rare earth element systematics in hydrothermal fluids. Geochimica et Cosmochimica Acta 53, 745–750.

Michard, A., Albarède, F., 1986. The REE content of some hydrothermal fluids. Chemical Geology 55, 51–60.

Moffett, J.W., 1990. Microbially mediated cerium oxidation in sea water. Nature 345, 421–423.

Murray, R.W., Buchholtz Ten Brink, M.R., Brumsack, H.J., Gerlach, D.C., Russ III, G.P., 1991. Rare-earth elements in Japan Sea sediments and diagenetic behavior of Ce/Ce*: results from ODP Leg 127. Geochimica et Cosmochimica Acta 55, 2453–2466.

Murray, R.W., Buchholtz Ten Brink, M.R., Gerlach, D.C., Russ III, G.P., Jones, D.L., 1992a. Interoceanic variation in the rare earth, major, and trace element depositional chemistry of chert: perspectives gained from the DSDP and ODP record. Geochimica et Cosmochimica Acta 56, 1897–1913.

Murray, R.W., Buchholtz Ten Brink, M.R., Gerlach, D.C., Russ III, G.P., Jones, D.L., 1992b. Rare-earth, major, and trace element composition of Monterey and DSDP chert and associated host sediment: assessing the influence of chemical fractionation during diagenesis. Geochimica et Cosmochimica Acta 56, 2657–2671.

Narayan, Y.R., 2003. A new Cenozoic foraminiferal biostratigraphy, paleocology (biofacies) and strontium isotope study of Shell Canada exploration wells from the Tofino Basin, offshore Vancouver Island, British Columbia. Ph. D. Thesis, Univ. Victoria, Victoria, Canada.

Nath, B.N., Bau, M., Rao, B.R., Rao, Ch.M., 1997. Trace and rare earth elemental variation in Arabian Sea sediments through a transect across the oxygen minimum zone. Geochimica et Cosmochimica Acta 61, 2375–2388.

Nitsche, H., 1990. Basic research for assessment of geologic nuclear waste repositories: what solubility and speciation studies of transuranium elements can tell us. Proc. Intl. Symp. On Sci. Basis for Nuclear Waste Management, Boston, MA.

Nozaki, Y., Alibo, D.-S., Amakawa, H., Gamo, T., Hasumoto, H., 1999. Dissolved rare earth elements and hydrography in the Sulu Sea. Geochimica et Cosmochimica Acta 63, 2171–2181.

Olivarez, A.M., Owen, R.M., 1989. REE/Fe variations in hydrothermal sediments: implications from the REE content of seawater. Geochimica et Cosmochimica Acta 53, 757–762.

Olmez, I., Sholkovitz, E.R., Hermann, D., Eganhouse, R.P., 1991. Rare earth elements in sediments off southern California: a new anthropogenic indicator. Environmental Science and Technology 25, 310–316.

Pattan, J.N., Higgs, N.C., Colley, S., Parthiban, G., 1995. Distribution of major, trace and rare-earth elements in surface sediments of the Wharton Basin, Indian Ocean. Chemical Geology 121, 201–215.

Piepgras, D.J., Jacobsen, S.B., 1992. The behavior of rare earth elements in seawater: Precise determination of variations in the North Pacific water column. Geochimica et Cosmochimica Acta 56, 1851–1862.

Pohlman, J.W., Kaneko, M., Heuer, V.B., Coffin, R.B., Whiticar, M., 2009. Methane sources and production in the northern Cascadia margin gas hydrate system. Earth and Planetary Science Letters 287, 504–512. doi:10.1016/j.epsl.2009.08.037.

Pourret, O., Davranche, M., Gruau, G., Dia, A., 2008. New insights into cerium anomalies in organic-rich alkaline waters. Chemical Geology 251, 120–127.

Rasmussen, B., Buick, R., Taylor, W., 1998. Removal of oceanic REE by authigenic precipitation of phosphaticminerals. Earth and Planetary Science Letters 164, 135–149.

Riedel, M., Collett, T.S., Malone, M.J., the Expedition 311 Scientists, 2005. Cascadia margin gas hydrates. Integrated Ocean Drilling Program Expedition 311 Preliminary Report. Integrated Ocean Drilling Program International Inc., Washington DC. doi:10.2204/iodp.pr.311.2005.

Riedel, M., Collett, T.S., Malone, M.J., the Expedition 311 Scientists, 2006. Proceedings of the Integrated Ocean Drilling Program Expedition, 311. Integrated Ocean Drilling Program International Inc, Washington DC. doi:10.2204/iodp.proc.311.2006.

Riedel, M., Collett, T.S., Malone, M.J., 2010. Expedition 311 synthesis: scientific findings. In: Riedel, M., Collett, T.S., Malone, M.J. (Eds.), Proceedings of the Integrated Ocean Drilling Program Expedition, 311. Integrated Ocean Drilling Program International Inc., Washington DC. doi:10.2204/iodp.proc.311.213.2010.

Ruhlin, D.E., Owen, R.M., 1986. The rare earth element geochemistry of hydrothermal sediments from the East Pacific Rise: examination of a seawater scavenging mechanism. Geochimica et Cosmochimica Acta 50, 393–400.

Schijf, J., De Baar, H.J.W., Millero, F.J., 1995. Vertical distributions and speciation of dissolved rare earth elements in the anoxic brines of Bannock basin, eastern Mediterranean Sea. Geochimica et Cosmochimica Acta 59, 3285–3299.

Sherrell, R.M., Field, M.P., Ravizza, G., 1999. Uptake and fractionation of rare earth elements on hydrothermal plume particles at 9°25′N, East Pacific Rise. Geochimica et Cosmochimica Acta 63, 1709–1722.

Sholkovitz, E.R., 1992. Chemical evolution of rare earth elements: fractionation between colloidal and solution phases of filtered river water. Earth and Planetary Science Letters 114, 77–84.

Sholkovitz, E.R., 1993. The geochemistry of rare earth elements in the Amazon River estuary. Geochimica et Cosmochimica Acta 57, 2181–2190.

Sholkovitz, E.R., Piepgras, D.J., Jacobsen, S.B., 1989. The pore water chemistry of rare earth elements in Buzzards Bay sediments. Geochimica et Cosmochimica Acta 53, 2847–2856.

Sholkovitz, E.R., Shaw, T.J., Schneider, D.L., 1992. The geochemistry of rare earth elements in the seasonally anoxic water column and porewaters of Chesapeake Bay. Geochimica et Cosmochimica Acta 56, 3389–3402.

Sholkovitz, E.R., Landing, W.M., Lewis, B.L., 1994. Ocean article chemistry: the fractionation of rare earth elements between suspended particles and seawater. Geochimica et Cosmochimica Acta 58, 1567–1579.

Smedley, P.L., 1991. The geochemistry of rare-earth elements in groundwater from the Carnmenellis area, southwest England. Geochimica et Cosmochimica Acta 55, 2767–2779.

Spivack, A.J., Kastner, M., Ransom, B., 2002. Elemental and isotopic chloride geochemistry and fluid Flow in the Nankai Trough. Geophysical Research Letters 29. doi:10.1029/2001GL014122.

Stanley Jr., J.K., Byrne, R.H., 1990. The influence of solution chemistry on REE uptake by *Ulva lactuca L.* in seawater. Geochimica et Cosmochimica Acta 54, 1587–1595.

Sugahara, H., Sugitani, K., Mimura, K., Yamashita, F., Yamamoto, K., 2010. A systematic rare-earth elements and yttrium study of Archean cherts at the Mount Goldsworthy greenstone belt in the Pilbara Craton: implications for the origin of microfossil-bearing black cherts. Precambrian Research 177, 73–87. doi:10.1016/j.precamres.2009.10.005.

Sverjensky, D.A., 1984. Europium redox equilibria in aqueous solution. Earth and Planetary Science Letters 67, 70–78.

Tachikawa, K., Jeandeal, C., Vangriesheim, A., Dupre, B., 1999. Distribution of rare earth elements and neodymium isotopes in suspended particles of the tropical Atlantic Ocean (EUMELI site). Deep-Sea Research I 46, 733–755.

Taylor, S.R., McLennan, S.M., 1985. The continental crust: its composition and evolution. Blackwell, Oxford.

Teichert, B.M.A., Torres, M.E., Bohrmann, G., Eisenhaue, A., 2005. Fluid sources, fluid pathways and diagenetic reactions across an accretionary prism revealed by Sr and B geochemistry. Earth and Planetary Science Letters 239, 106–121.

Torres, M.E., Teichert, B.M.A., Tréhu, A.M., Borowski, W., Tomaru, H., 2004. Relationship of pore water freshening to accretionary processes in the Cascadia margin: fluid sources and gas hydrate abundance. Geophysical Research Letters 31. doi:10.1029/2004GL021219.

Torres, M.E., Tréhu, A.M., Cespedes, N., Kastner, M., Wortmann, U.G., Kim, J.-H., Long, P., Malinverno, A., Pohlman, J.W., Riedel, M., Collett, T., 2008. Methane hydrate formation in turbidite sediments of northern Cascadia, IODP Expedition 311. Earth and Planetary Science Letters 271, 170–180. doi:10.1016/j.epsl.2008.03.061.

Wyndham, T., McCulloch, M., Fallon, S., Alibert, C., 2004. High-resolution coral records of rare earth elements in coastal seawater: biogeochemical cycling and a new environmental proxy. Geochimica et Cosmochimica Acta 68, 2067–2080.

Zhang, J., Liu, C.-Q., 2004. Major and rare earth elements in rainwaters from Japan and East China Sea: natural and anthropogenic sources. Chemical Geology 209, 315–326.

Ziegler, C.L., Murray, R.W., Hovan, S.A., Rea, D.K., 2007. Resolving eolian, volcanogenic, and authigenic components in pelagic sediment from the Pacific Ocean. Earth and Planetary Science Letters 271 (254), 416–432. doi:10.1016/j.epsl.2006.11.049.